Multi-frequency sub-1 GHz radio tomographic imaging in a complex indoor environment

2017 International Conference on Indoor Positioning and Indoor Navigation (IPIN), 18-21 September 2017, Sapporo, Japan

Multi-Frequency Sub-1 GHz Radio Tomographic Imaging in a Complex Indoor Environment

Stijn Denis, Rafael Berkvens, Glenn Ergeerts, and Maarten Weyn
University of Antwerp - imec, IDLab, Faculty of Applied Engineering
Groenenborgerlaan 171, Antwerp, Belgium
stijn.denis@uantwerpen.be

***Abstract*—Unlike most currently available localization systems, tagless localization technologies do not require a target to wear a passive or active hardware device. Radio Tomographic Imaging (RTI) is one such technique, which operates based on the use of a tomographic radio frequency (RF) sensor network. The majority of RTI-systems communicate using a single frequency band: 2.4 GHz. The use of sub-1 GHz frequencies within RTI could potentially provide important benefits regarding energy efficiency, accuracy in complex indoor environments and size of the environments in which a system can be installed. We deployed a combined 433 MHz and 868 MHz RF sensor network in a complex indoor environment and performed localization when a human individual was present in the environment. Two different RTI-algorithms were investigated: a Bayesian-based method we developed earlier and an adaptation of an existing 2.4 GHz technique based on fade level. Both methods turned out to be capable of accurately locating individuals with a median error lower than 1 meter. This proves the feasibility of using a combination of sub-1 GHz frequencies in RTI for indoor localization in complex environments.**

***Keywords*—radio tomographic imaging, sub-1 GHz, device-free localization, tagless localization, tomographic sensor network**

I. Introduction

Over the past decade, there has been growing interest in the development of device-free or tagless localization techniques. These techniques, unlike most currently available localization systems, do not require the person or object to be located to wear a passive or active hardware device (a tag) [1]. A position is estimated based solely on the impact that the physical presence of the entity has on its environment. Depending on the application, the absence of this requirement can be an important advantage. A classic example is tracking of the elderly [2], for whom the constant wearing of a tag can be perceived as stigmatizing. Other common applications include security systems and systems employed by emergency services when people in danger need to be located quickly [3].

Techniques based on radio frequency signals comprise an intriguing domain within device-free localization. Through-the-wall ultra-wideband (UWB) imaging systems based on reflection and refraction of a transmitted signal by the target (analogous to radar) are commercially available, though tend to be expensive [4]. The use of a network of low-cost RF-transceivers which measures the characteristics of transmissions between the nodes is a potentially cheaper alternative. Passive Radio Mapping [5] is a technique which utilizes such a network. It is a fingerprinting algorithm in which the fingerprint database consists of the RSS-values of the communication links between static nodes in the environment while an individual is present. High accuracy in large environments can be obtained without the need for any specialized infrastructure, but it quickly becomes harder and more time intensive to construct a fingerprint database if multiple people are present in the environment.

Radio Tomographic Imaging (RTI) [6] also makes use of an RF sensor network. Rather than relying on a fixed reference database, an RTI-system attempts to determine which locations within the environment were most likely responsible for measured RSS-changes of the communication links. The basic algorithm takes as input a list of RSS-differences between the current measurement and an earlier calibration measurement when the environment did not contain any targets and creates an attenuation image. This image is a representation of the environment in which the value of each pixel indicates the average attenuation a communication link will experience when its line-of-sight traverses the corresponding location. Pixels with a high amount of attenuation are assumed to be more likely to contain locatable entities.

Several variations and improvements of the basic RTI-technique do exist. In variance based RTI (VRTI) [3], a windowed variance of the n most recent RSS-link measurements is used as input to the algorithm. This eliminates the need for an earlier calibration step and paves the way for the use of RTI in emergency applications. A multi-channel approach where the nodes communicate on multiple frequency channels is introduced in [7]. An advanced multi-tracking model can lead to accurate simultaneous tracking of up to 4 individuals [8]. [9] proposes an RTI-technique in which the impact of each RSS-link on the final attenuation image is dependent on fade level. This model will later be explained in more detail in section III.

In the majority of current Radio Tomographic Imaging systems, the nodes communicate using 2.4 GHz signals. The use of multiple sub-1 GHz frequency bands in a single RTI-system could potentially solve several shortcomings of the technique. Evaluation of the localization accuracy of a combined 868 MHz/2.4 GHz system in [10] shows a root mean square error (RMSE) of 26 cm when locating a single individual in an indoor office environment. Interestingly, the results show that the single-frequency 868 MHz system obtains more accurate results than the 2.4 GHz system if no extra filtering techniques

are applied. The larger wavelengths of sub-1 GHz signals makes it more difficult for them to be influenced by human presence, thus one would generally expect the opposite case to be true. However, this same aspect also tends to make them less susceptible to multi-path effects caused by a multitude of static objects, which the RTI-algorithm interprets as noise. This can be an important advantage in complex environments.

Furthermore, the increased communication range offered by sub-1 GHz frequencies could play an important role regarding the size of the environments in which a system can be installed. Recently, interest has been shown in the use of RTI-systems in large scale outdoor environments. A 2.4 GHz system was deployed in a 35 m x 60 m heavily forested area in [11]. The authors suggest an analysis of the performance of different frequency bands such as 433 and 900 MHz as a potentially interesting future research direction.

Finally, the use of sub-1 GHz frequencies could enable the creation of more energy-efficient RTI-systems using existing low-power communication solutions. In all experiments described in this paper, our nodes communicate using the DASH7-Alliance Protocol (D7AP) [12], an open source low-power industry alliance standard for wireless sensor and actuator communication over the unlicensed 433, 868 and 915 RF bands.

The first step in researching multi-frequency sub-1 GHz Radio Tomographic Imaging consists of determining the suitability of these frequencies for RTI. In [13], we demonstrated the feasibility of combining only sub-1 GHz frequencies in a single system. Basic RTI-systems for 433 MHz and 868 MHz were deployed in an open indoor environment of 60 m^2. The resulting attenuation maps when a stationary individual was present in the environment were combined using a probabilistic method, leading to a root mean square error (RMSE) of 54 cm.

In this paper, we continue our investigation into the use of these non-traditional RTI bands for a more complex environment. Compared to our previous work, We implement and validate a 433- and 868 MHz tomographic sensor network in a much larger, 2-room office environment. Furthermore, the network collects RSS-data when one *or* two human individuals are present. This enables us to investigate the feasibility of locating multiple individuals within multi-frequency RTI. Finally, the data is analyzed using two different RTI-techniques: the probabilistic approach we used in [13] and a sub-1 GHz adaptation of an existing fade level-based spatial RTI-model presented in [9]. The results are then compared.

The remainder of this paper is structured as follows: in section II several key concepts of Radio Tomographic Imaging are explained. Section III contains the methodology we use regarding the implementation of the tomographic sensor network as well as an explanation of the two RTI-techniques. The experiments we performed and the obtained results thereof are detailed in section IV. Finally, a conclusion and an overview of potentially interesting future research directions are presented in section V.

II. Radio Tomographic Imaging

Radio Tomographic Imaging is a tagless localization technique based on the use of a tomographic RF-sensor network. The nodes of this network repeatedly transmit and receive radio frequency signals, thereby creating a number of communication links whose lines-of-sight traverse an environment. The presence of a locatable entity in this environment will influence the received signal strengths of the links. Based on this influence, an attenuation map is created which depicts the average attenuation a link will experience when crossing that pixel. During the next step, a positioning technique is applied in order to obtain actual location estimates. In the next few paragraphs, we will describe the workings of a basic shadowing-based RTI-algorithm as defined in [6] and [9]. This algorithm will be used all throughout the rest of the paper.

First, we create a grid representation of the environment in which we wish to perform localization by dividing it into N amount of equally sized pixels. Next, RSS-differences between a live measurement and a set of earlier calibration measurements when the environment did not contain any targets are saved in a vector $\boldsymbol{y}$ of size M, with M being the total amount of communication links in the sensor network. A weighting matrix W of size M x N is then created. This matrix quantifies the relationship between each link and what part of the environment it provides information about. Each row of this matrix defines the different weights of all pixels in relation to a specific link. For the final step, we define a vector $\boldsymbol{x}$ of size N which contains the attenuation image we wish to obtain. Vector $\boldsymbol{y}$ is then described as

$$\mathbf{y} = W\mathbf{x} + n \tag{1}$$

with n being a noise vector. The goal of RTI is to calculate this vector x. Given that this is an ill-posed problem, a unique correct solution does not exist and has to be approximated. In shadowing-based RTI, a maximum a posteriori (MAP) approximation is used, which leads to the following formula:

$$\mathbf{x}_{MAP} = (W^T W + C_x^{-1}\sigma_N^2)^{-1} W^T \mathbf{y} \tag{2}$$

x_{MAP} represents the desired approximation of the image vector. W still represents the M x N weighting matrix. Each element of W is calculated according to this formula:

$$W_{ij} = \begin{cases} 1/\sqrt{(d_i)} & \text{if } d_{ij}(1) + d_{ij}(2) < d_i + \lambda \\ 0 & \text{otherwise} \end{cases} \tag{3}$$

with d_i representing the distance between the nodes which define link i. $d_{ij}(1)$ and $d_{ij}(2)$ represent the distance between these nodes and a pixel j. As long as a pixel lies within an ellipse which has the two link nodes as its foci and is defined by the parameter λ, the corresponding weighting matrix value will be inversely proportional to the square root of the distance between the nodes. If it lies outside of the ellipse it will be equal to zero.

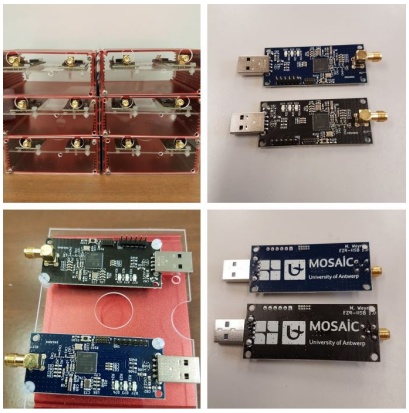

Fig. 1: RTI nodes and transceivers

C_x is a covariance matrix which is used for regularization. Each value of this matrix is calculated using an exponential spatial decay model:

$$[C_x]_{kl} = \sigma_x^2 * e^{-d_{kl}/\delta_c} \tag{4}$$

d_{kl} represents the distance between pixels k and l. σ_x^2 is the pixel variance and δ_c is a space correlation constant which determines the overall smoothness of the resulting x_{map}. An overview of other potential regularization techniques which can be used for RTI is given in [14].

Finally, σ_N^2 is a regularization parameter.

The formula in 2 can be rewritten as:

$$x_{MAP} = \Pi y \tag{5}$$

This projection matrix Π can be calculated when the system is offline. This theoretically reduces the computational complexity for a real-time RTI-system to a single matrix multiplication. In practice, however, it can be necessary to update the projection matrix if there are communication issues in the network. The (temporary) disappearance of links necessitates changing the weighting matrix which leads to the recalculation of the projection matrix.

III. Methodology

A. Construction of a tomographic sensor network

The tomographic sensor network we use in our experiments contains 39 battery-powered nodes. Each node consists of 2 (433 MHz and 868 MHz) self-developed EZR-USB RF-transceivers placed next to each other within a casing. Several nodes are shown in figure 1. As mentioned earlier, communication occurs by using the DASH7-Alliance Protocol. The entire sensor network is essentially divided into two separate networks based on frequency band which operate independently of each other.

In order to ensure that communication within the network occurs in an orderly fashion with a minimal amount of collisions, a new communication schedule was developed. This communication schedule is an important improvement upon the scheme which we used earlier in [13] (which was originally based on a protocol presented in [10] and [15]) due to its flexibility and stability.

There are three types of nodes: 37 regular nodes, 1 controller node and 1 configuration node. The controller node regulates the communication within the network and passes on the RSS-data to a laptop to which it is connected. The configuration node is responsible for answering requests of the controller and regular nodes regarding a set of network parameters. Finally, the regular nodes each in turn broadcast an RTI-packet which is received by the other regular nodes and the controller node. The RSS with which these packets are received are used to determine the RSS-values of the communication links.

The setup of the network is described in the following paragraphs.

First, the configuration node is placed in the environment and powered on. It is very important that this node is in range of and can reliably communicate with all other nodes.

Next, the controller node is installed near the edges of the environment and connected to a laptop with a serial communication link. On boot, it repeatedly broadcasts a *configuration_request* message until it receives a *configuration_response* from a configuration node in range. This configuration message contains an *rti_id* and 5 network parameters: *wtime*, *txtime*, *main_channel*, *main_eirp* and *network_size*:

- *rti_id* is the unique id of each node which determines the order in which each RTI-node is allowed to broadcast a packet. The configuration node contains an internal list linking the hardware id of each node to an *rti_id*. For the controller node, the *rti_id* will always be 255.
- *wtime* is the time between the transmission of two subsequent RTI-packets by the regular nodes in milliseconds.
- *txtime* is the maximum allotted transmission time for a regular node to send a packet.
- *main_channel* is the id of the frequency channel in which the regular nodes will communicate with each other. Per the D7AP version 1.1 specifications described in [16], there are 32 channels for 868 MHz and 8 channels for 433 MHz normal-rate communication with each channel having a maximum bandwidth of 180 kHz. It is important to note that *main_channel* only defines the channel id which the regular and controller nodes will use for RTI-communication. All configuration-related communication in the network occurs on a separate, fixed channel known to all nodes in advance.
- *main_eirp* defines the equivalent isotropically related power (EIRP) with which the nodes will transmit.
- *network_size* defines the total number of regular nodes within the network.

During the next step, the regular nodes are deployed inside the environment at specifically chosen locations and powered. On boot, they broadcast configuration request messages until they receive a response from the controller node. Upon receiving the response, they start to listen for instructions by the controller node on the channel defined by *channel_id*. Once all

nodes have received their configuration parameters, the system is now ready to be activated and collect RSS-data.

The system can be activated by the laptop sending an *rti_start* command to the controller through the serial communication link. This leads to the following steps:

1) The controller broadcasts a cycle start message to all regular nodes.
2) When a regular node receives the start message, it schedules the task of broadcasting an *rti_message* at *wtime* * *rti_id* milliseconds in the future. When a node receives an *rti_message*, it will save the RSS-value of this communication instance in an internal list. Once the time has arrived for the previously receiving node to transmit, the *rti_message* it broadcasts will contain this list. The utility of an *rti_message* is therefore twofold: it serves both as a way to determine the RSS-values of the communication links as well as a way to relay this information to the controller node.
3) The controller node receives the *rti_messages* and sends the RSS-data therein to the laptop through the serial communication link. Once *wtime* * *network_size* amount of milliseconds (plus a slight amount of buffer time to account for clock drift) has passed, the controller will send a new cycle start message and the entire process will begin anew. If the controller receives an *rti_stop* message from the laptop, it will merely complete the current cycle and not send a new start message.

It is possible that during the course of a cycle, a node might encounter an error and crash. In this case, the node will restart itself and broadcast a configuration request in exactly the same manner as in the setup phase. The configuration node will respond and the regular node is again able to participate in the next RTI-cycle. This instance of configuration-related communication does not interfere with the currently ongoing RTI-cycle due to the fact that it occurs on a different channel. During the missed cycles, the other nodes will not have received any messages from the crashed node. Their internal RSS-lists will contain the value 0 for this node, which passes on the problem to the RTI-algorithm on the laptop.

If one wishes to change the configuration parameters of the network, only the firmware of the configuration node needs to be updated. The laptop can then send an *update_config* command which causes the controller to broadcast a *change_config* message. This message prompts the regular nodes to send *configuration_requests*. Finally, the controller will also send a *configuration_request*.

All of the RSS-data which is collected in this tomographic sensor network is sent to the laptop connected to the controller. There it is shaped into the form of an L x L RSS-matrix for each cycle with L being the total number of nodes. The data is then used as input to a Radio Tomographic Imaging algorithm. As mentioned earlier, we will compare two different RTI-techniques: a Bayesian-based RTI method [13] and an adaptation of an existing fade-level based model [9].

B. Bayesian-based RTI method

Because there is two-way communication between the nodes, the matrices we receive from the tomographic sensor network generally contain two (non-zero) RSS-values for each link. We define the RSS-value of a communication link as the average of these two values and save them to a link vector. If one of these values is equal to zero, the remaining one is used. Both values being equal to zero indicates that there is no information available regarding that link during a certain cycle. A 0 will be written to the corresponding location in the link vector.

Calibration link vectors are created based on measurements when the environment did not contain any locatable entities. These are averaged in order to obtain a reference vector. A vector y is obtained by calculating the difference between a link vector when entities were present and the reference vector. If a 0 is detected in the link vector, the corresponding link is not included in the y-vector. This vector y is then used in the formula given in (2). The parameters used for the creation of the covariance matrix C_x and the weighing matrix W were chosen empirically. It is important to note that W is updated in order to take into account the links that were removed.

All of the aforementioned steps are performed for both 433 MHz- and 868 MHz-data which was captured at approximately the same time. This results in two separate attenuation images which need to be combined. Each pixel of this image indicates the average attenuation a link will experience when traversing that location and is therefore a value which is expressed in dB. We will convert these attenuation images into probability images where the value of a pixel directly tells us the probability of an entity being present in the corresponding location. This enables us to directly combine multiple images by element-wise multiplication.

In order to do so, we make use of training data. Several attenuation images are created where a single human individual was present in the environment in known locations. The values of the pixels immediately surrounding the true locations where the individual was standing are fitted to a normal distribution. This distribution is interpreted as $P(x_i \mid A_i)$, the likelihood that the value of pixel i is equal to x_i provided that i contains a human presence. Similarly, a normal distribution is fitted to the values of all other pixels in the image where no individual was present: $P(x_i \mid \overline{A_i})$. These two distributions can then be used in Bayes Theorem in order to determine $P(A_i \mid x_i)$, the probability of human presence depending on the value of the corresponding pixel in the attenuation image:

$$P(A_i \mid x_i) = \frac{P(x_i \mid A_i)P(A_i)}{P(x_i \mid \overline{A_i})P(\overline{A_i}) + P(x_i \mid A_i)P(A_i)} \quad (6)$$

$P(A_i)$ is determined in an empirical manner. This formula is applied to each pixel of the generated attenuation images and the resulting probabilistic images for 433 MHz and 868 MHz are combined.

C. Fade-level based method

There are three important differences between the probabilistic technique described in the previous section and the fade level-based spatial weight model. First, the parameter λ is no longer a constant for each link. This parameter is used in the construction of the weighting matrix to determine for each link what parts of the environment it can be influenced by as described in equation (3). Instead, we create an exponential model which describes λ as a function of link fade level. Second, the value of each pixel in the weighting matrix within the ellipse is now given by $1/A_l$, with A_l being the surface area of the ellipse. Third, vector $\boldsymbol{y}$ is transformed from an RSS-difference vector into a probabilistic vector which is then used in the main RTI-formula. This means that the resulting x_{map} will already be probabilistic and easy to combine with other vectors generated by different frequency bands.

1) Fade Level-Based Spatial Weight Model: We define fade level as the difference between the expected RSS of a link according to an RF propagation model and the measured RSS of that link in an environment which does not contain any human presence:

$$F_l = \overline{r_l} - P(d) \tag{7}$$

with $\overline{r_l}$ being the average RSS of link l and $P(d)$ representing a propagation model as a function of the distance d between the nodes. In this paper, we will use the Friis transmission equation [17] as our model:

$$P_r = P_t + G_t + G_r + 20\log_{10}(\frac{\lambda}{4\pi d}) \tag{8}$$

P_r is the received power at a certain location and P_t is the output power of the transmitter. G_t and G_r are the antenna gains at respectively the transmitter and the receiver. λ is the wavelength of the center frequency and d is the distance between the antenna's.

We measure the RSS-values within the tomographic sensor network when the environment does not contain human presence and use equations (7) and (8) to calculate the fade level of each link. We then sort our links into 18 different categories based on their fade level so that each category contains the same amount of links. Next, we perform a series of RF-measurements when a human individual is present in the environment in a known location. The measurements of each link belonging to a certain category are all collected in a single bin. We then consider the 5th percentile of measurements where the largest increase in RSS-value occurred and the 5th percentile of measurements where the largest decrease in RSS-value occurred (when compared to a calibration measurement). We calculate the minimum excess path length for each value belonging to these measurement sets. This is defined as the value of λ with which the individual in the environment is right on the perimeter of the corresponding ellipse. We denote the minimum excess path length values when the RSS-values strongly increased as λ^+, when the RSS-values strongly decreased as λ^-. We then determine the median values of these two sets.

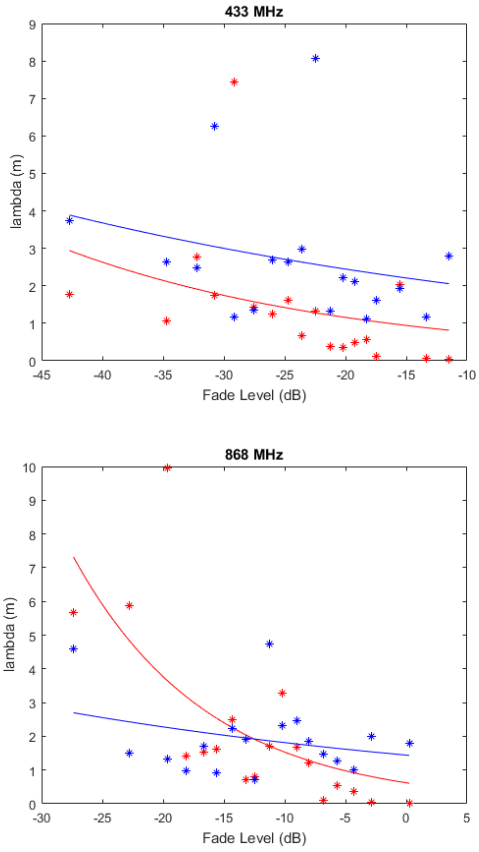

Fig. 2: λ^-(blue) and λ^+(red) as a function of fade level for 433 MHz and 868 MHz.

This entire process is repeated for each fade level category. The resulting median λ^+ and λ^- are shown in figure 2 for both 868 MHz and 433 MHz. They are fitted to exponential decay models. Interestingly, this differs from the 2.4 GHz model presented in [9], where λ^+ could be fitted to an exponential growth model. In both cases the difference in λ^+ depending on fade level is rather small, however, especially when compared to λ^- for 868 MHz.

We now have a way to calculate a unique λ for each link based on fade level and sign of the measured RSS-value when the system is active. The next step consists of developing a model which is able to convert the RSS-difference vector $\boldsymbol{y}$ into a probability vector.

2) Probabilistic link vector: First, we divide the measurements we obtained in the previous section within each bin into 100 sub-bins. A sub-bin consists of measurements which have roughly the same RSS-change value. We then approximate for each sub-bin the probability that the individual was present outside of the corresponding ellipse. This approximation is performed for the sub-bins of all bins. In figure 3, the probabilities are shown for all sub-bins of fade level bin $F \in [-13.71, -12.79]$ (868 MHz) and fade level bin $F \in [-25.33, -24.32]$ (433 MHz). The results can be

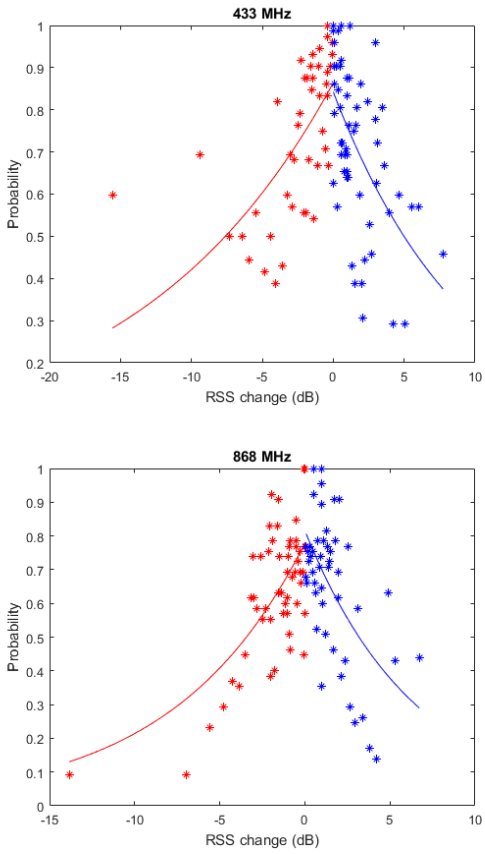

Fig. 3: Probability of a person being outside the link ellipse in function of RSS change. Negative RSS-changes in red, positive RSS-changes in blue.

fitted to an exponential growth model for RSS-decreases and an exponential decay model for RSS-increases. This provides us with a model to calculate the probability of an individual being present within the ellipse of a link in function of the measured RSS-change for each bin.

In [9], a generalized model is constructed for all bins which is validated for multiple environments. The focus of this paper is the examination of the feasibility of using multi-frequency sub-1 GHz systems in complex indoor environments and not the construction of an advanced generalized RTI-model. Therefore, this lies outside of the scope of this paper. In our experiments, we will use a model with different parameters for each link bin.

We can now use these models to convert each value within our RSS-difference vector $\boldsymbol{y}$ into a probability and plug the result into formula (2). As mentioned earlier, the resulting x_{map} image vectors will already be probabilistic and no extra steps are necessary to ensure that they can be combined by element wise multiplication.

D. Positioning

The final step of RTI-localization consists of determining the number of entities in the environment and their corresponding locations based on the calculated x_{map} vectors. A simple thresholding method is used in combination with a weighted centroid based approach. An empirically determined threshold T is applied to the entire image vector. The weighted centroids of the still remaining clusters are then determined, provided that the size of the cluster is equal to or larger than another empirically determined threshold t. The coordinates of the weighted centroids are considered to be the estimates of the system regarding the true location of human entities in the environment.

TABLE I: RTI Image Reconstruction Parameters

Parameter	Bayesian Method	Fade level Method
p (pixel width)	0.25 m	0.25 m
σ_s^2	0.4 dB^2	1 dB^2
σ_N^2	10	20
δ_c	4 pixels	0.05 pixels

IV. Experimental Setup & Results

We deploy a tomographic sensor network in a complex indoor office environment of size 14.29 m x 8.76 m. It consists of two rooms separated by a solid wall and connected by a hallway. The nodes are placed at a height of 1 meter alongside the walls within the environment. Next, we select 45 locations within the environment where human individuals will be present. We divide the locations in each room semi-randomly into locations used as training data and locations used for evaluation of the system. Around 55 % of locations in each room are training locations.

A schematic overview of the environment is provided in figure 4. The lower left part of the environment, even though it is traversed by a (limited) amount of links, was not part of the experiment and is therefore grayed out.

A. Singular Human Presence

Calibration data is collected by running the tomographic sensor network for 15 minutes when there are no human individuals within the environment and averaging the RSS-values of the resulting cycles. We then perform the steps described in section III when a single person was present for the given test and training locations. Both the Bayesian probabilistic method as well as the fade level-based method are used. Just as in [9], the main RTI image reconstruction parameters that we selected are provided in table I. We do so for both methods.

If the RTI-system does not detect any human presence, it is listed as a false negative. If it detects more than one person being present, it is a false positive. We determine the location error of the remaining cases. Location error is defined as the distance between the estimated location of the individual and their actual location. 4 RTI-cycles of 21 test locations are used as input, giving us a total of 84 data sets. The results are provided in table II. In figure 5, a cumulative distribution function of the location errors is shown for both techniques.

It appears from the results that the Bayesian-based technique is more accurate and suffers from less outliers. However, it correctly assesses the correct amount of people in the

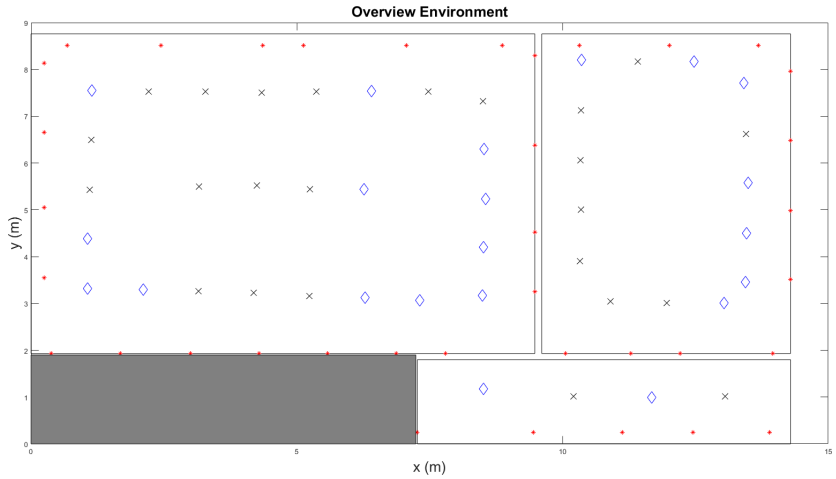

Fig. 4: Schematic overview of the test environment. Nodes are indicated by the red asterisks, training locations by the black crosses and test locations by the blue diamonds.

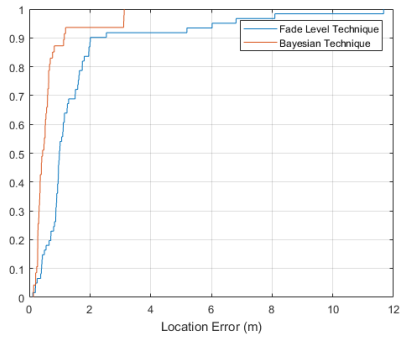

Fig. 5: Cumulative distribution function for 84 data sets.

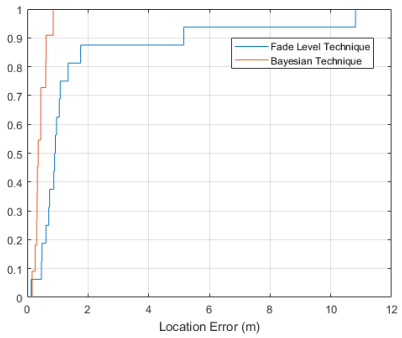

Fig. 6: Cumulative distribution function for 21 data sets.

TABLE II: Localization error for 84 data sets

	Bayesian Method	Fade level Method
false positives	4	9
false negatives	33	14
mean	0.65 m	1.59 m
median	0.44 m	0.99 m
standard deviation	0.70 m	1.98 m
75th percentile	0.64 m	1.62 m
rmse	0.95 m	2.53 m

environment far less often than the fade-level based technique. We performed the same analysis of the data after averaging the cycles for each test location, providing us with only 21 data sets. Results are given in table III and figure 6.

TABLE III: Localization error for 21 data sets

	Bayesian Method	Fade level Method
false positives	1	1
false negatives	9	4
mean	0.43 m	1.75 m
median	0.36 m	0.91 m
standard deviation	0.20 m	2.67 m
75th percentile	0.57 m	1.21 m
rmse	0.47 m	3.12 m

The results for the Bayesian method are not impacted significantly, whereas the fade-level method has (relatively speaking) slightly less false positives and negatives than in the previous case. It is much more susceptible to outliers, however, as can clearly be seen by the sharply increased standard deviation. Nevertheless, the median error remains slightly under 1 m.

B. Double Human Presence

We repeat the experiment with two human individuals in the environment. The same training data is used as in the previous section (with one person present in the environment), but the new test data consists of measurements taken when 2 people were present at 19 random combinations of 2 possible locations. It often occurs that when those 2 people are standing close to each other, only one (large) cluster is created in the resulting image vector. A more thorough positioning system which can identify these 'superclusters' is outside of the scope of this paper. Therefore, when determining false negatives, we will not count a single cluster when two people are present in the environment as a false negative provided that these two people are no further than 2 meters apart. We will then define the location errors for both individuals as

TABLE IV: Localization error for 76 data sets for 2 people present in the environment

	Bayesian Method	Fade level Method
false positives	6	7
false negatives	24	34
superclusters	14	16
mean	2.20 m	2.50 m
median	0.62 m	1.49 m
standard deviation	2.86 m	2.54 m
75th percentile	3.29 m	3.39 m
rmse	3.60 m	3.55 m

the separate distances between the 2 true locations and the weighted centroid of the cluster. Results are given in table IV for 19 x 4 = 76 data sets.

Unsurprisingly, the location error increases when there are multiple people present in the environment. The median error of the Bayesian technique remains lower than 1 meter however. Interestingly, we see that the fade-level method has the most false positives and false negatives now. When manually looking through the resulting x_{map} images, a potential explanation for the large amount of false negatives can be found. It happens quite often that a single, very large supercluster is generated even when the nodes are farther apart than 2 meter from each other.

There are still some improvements necessary in order to be able to reliably track multiple individuals within the environment. Nevertheless, it is clear that locating multiple individuals is possible with a combined sub-1 GHz RTI-system.

V. Conclusion & Future Work

We have successfully deployed a Radio Tomographic Imaging system which only utilizes Sub-1 GHz Frequencies in a complex indoor environment. Both the Bayesian system as well as the fade level based system were capable of locating a single person with a median error lower than 1 meter. We have now demonstrated that it is feasible to use a multi-frequency sub-1 GHz RTI-system in a complex indoor environment. Both systems have their shortcomings, however. The Bayesian method is consistently very accurate but is sensitive to false negatives. The fade level-based method on the other hand is much less accurate and suffers from multiple outliers, but manages to correctly assess the amount of individuals present in the environment more often. We suspect that potential solutions to these problems include parameter optimization, the use of a more detailed RF propagation model for the fade level system, the use of a more sophisticated positioning algorithm and the use of a motion model when tracking moving targets. A combination of both systems is also an interesting research topic that will be looked at in the future. Additionally, we will look into the development of a true general adaptation of the model presented in [9] for 433 MHz and 868 MHz regardless of environment.

All of the aforementioned improvements will be combined into an advanced multi-frequency RTI system, which will then be deployed in specific environments where it could potentially provide important advantages when compared to a single-frequency 2.4 GHz system. Examples include very complex indoor environments with a large amount of multipath effects and large-scale outdoor environments.

VI. Acknowledgements

Part of this research was funded by the Flemish FWO SBO S004017N IDEAL-IoT (Intelligent DEnse And Longe range IoT networks) project.

References

[1] M. Youssef, M. Mah, and A. Agrawala, "Challenges: device-free passive localization for wireless environments," in *Proceedings of the 13th annual ACM international conference on Mobile computing and networking*. ACM, 2007, pp. 222–229.

[2] O. Kaltiokallio, M. Bocca, and N. Patwari, "Follow@ grandma: Long-term device-free localization for residential monitoring," in *Local Computer Networks Workshops (LCN Workshops), 2012 IEEE 37th Conference on*. IEEE, 2012, pp. 991–998.

[3] J. Wilson and N. Patwari, "See-through walls: Motion tracking using variance-based radio tomography networks," *Mobile Computing, IEEE Transactions on*, vol. 10, no. 5, pp. 612–621, 2011.

[4] "Camero Tech," "http://www.camero-tech.com/", Page retrieved on 15/05/2017.

[5] M. Seifeldin, A. Saeed, A. E. Kosba, A. El-Keyi, and M. Youssef, "Nuzzer: A large-scale device-free passive localization system for wireless environments," *IEEE Transactions on Mobile Computing*, vol. 12, no. 7, pp. 1321–1334, 2013.

[6] J. Wilson and N. Patwari, "Radio tomographic imaging with wireless networks," *IEEE Transactions on Mobile Computing*, vol. 9, no. 5, pp. 621–632, 2010.

[7] O. Kaltiokallio, M. Bocca, and N. Patwari, "Enhancing the accuracy of radio tomographic imaging using channel diversity," in *Mobile Adhoc and Sensor Systems (MASS), 2012 IEEE 9th International Conference on*. IEEE, 2012, pp. 254–262.

[8] M. Bocca, O. Kaltiokallio, N. Patwari, and S. Venkatasubramanian, "Multiple target tracking with rf sensor networks," *IEEE Transactions on Mobile Computing*, vol. 13, no. 8, pp. 1787–1800, 2014.

[9] O. Kaltiokallio, M. Bocca, and N. Patwari, "A fade level-based spatial model for radio tomographic imaging," *IEEE Transactions on Mobile Computing*, vol. 13, no. 6, pp. 1159–1172, 2014.

[10] A. Fink, T. Ritt, and H. Beikirch, "Redundant radio tomographic imaging for privacy-aware indoor user localization," in *Indoor Positioning and Indoor Navigation (IPIN), 2015 International Conference on*. IEEE, 2015, pp. 1–7.

[11] C. Alippi, M. Bocca, G. Boracchi, N. Patwari, and M. Roveri, "Rti goes wild: Radio tomographic imaging for outdoor people detection and localization," *IEEE Transactions on Mobile Computing*, vol. 15, no. 10, pp. 2585–2598, 2016.

[12] M. Weyn, G. Ergeerts, R. Berkvens, B. Wojciechowski, and Y. Tabakov, "Dash7 alliance protocol 1.0: Low-power, mid-range sensor and actuator communication," in *Standards for Communications and Networking (CSCN), 2015 IEEE Conference on*. IEEE, 2015, pp. 54–59.

[13] S. Denis, R. Berkvens, G. Ergeerts, B. Bellekens, and M. Weyn, "Combining multiple sub-1 ghz frequencies in radio tomographic imaging," in *Indoor Positioning and Indoor Navigation (IPIN), 2016 International Conference on*. IEEE, 2016, pp. 1–8.

[14] J. Wilson, N. Patwari, and F. G. Vasquez, "Regularization methods for radio tomographic imaging," in *2009 Virginia Tech Symposium on Wireless Personal Communications*, 2009.

[15] S. Savazzi, M. Nicoli, and M. Riva, "Radio imaging by cooperative wireless network: Localization algorithms and experiments," in *Wireless Communications and Networking Conference (WCNC), 2012 IEEE*. IEEE, 2012, pp. 2357–2361.

[16] *D7A Specification 1.1 Wireless Sensor and Actuator Network Protocol*, DASH7 Alliance, 2016, version 1.1.

[17] A. S. Joseph, "Radiometry and the friis transmission equation," *Technical Paper*, 2005.